Seabed classification using normal incidence backscatter measurements in the 1-10 kHz frequency band

P. C. Hines[1], G. J. Heald[2,3]

[1] Defence Research Establishment Atlantic, P.O. Box 1012, Dartmouth, NS, B2Y 3Z7, Canada. hines@drea.dnd.ca
[2] University of Bath, Claverton Down, Bath, BA2 1AY, UK.
[3] DERA, Bincleaves, Newton Rd, Weymouth, Dorset, DT4 8UR, UK. gjheald@dera.gov.uk

Abstract

It has been established that the 1st and 2nd seabed returns from a monostatic echosounder can be used as a seabed classification tool. Typically these systems operate in the range of several tens of kHz so that bottom roughness at the seabed interface is the dominant scattering mechanism. In this paper we extend the model to lower frequencies; in this context lower frequency implies that scatter from the sub-bottom must be accounted for in the model. Preliminary results indicate that volume scatter should provide an additional discrimination tool without significantly corrupting the seabed information contained in the interface scatter returns. Not surprisingly, this improvement comes at the cost of further complicating the model.

1. Introduction

Acoustic scatter from the seabed has been – and continues to be – a subject of substantial interest to the underwater acoustics community. This is not surprising since the scattered energy often serves as the noise background against which signals of interest must be measured. The literature contains a plethora of articles on the modeling and measurement of acoustic scatter from the seabed (c.f. [1-3] and the references therein). It is not the intent of this introduction to review this vast subject as an end in itself but rather as a means to an end. That is to say, we shall consider the scattered field as it pertains to the subject of acoustic inversion.

Acoustic inversion can be loosely defined as the utilization of acoustic techniques to measure non-invasively, the geophysical properties of the seabed. This rapidly growing research area spans an enormous frequency band, from a few Hz to hundreds of kHz. At the lowest frequencies it is used in the seismic industry to explore for sites likely to be rich in oil and gas deposits. At frequencies of hundreds of Hz several inversion techniques evolved from Matched Field Processing (MFP) in which one localized a source by employing knowledge of the receiver location and the environment [4]. This led to acoustic inversion whereby the search was carried out not only for source position but also for a set of geophysical parameters such as wave speed, density, and sediment layer thickness [5, 6]. In the low kHz frequencies Holland and Osler [7] employed a joint time-frequency approach to perform high-resolution geoacoustic inversion which addresses the uniqueness problem typical of many inversion techniques. For additional background on acoustic inversion across this fairly wide frequency band, the interested reader is referred to the collection of papers contained in [8] and [9].

Much of the work at low and mid-frequencies concentrates on acoustic inversion for geotechnical and geophysical properties. In contrast, research at the upper end of the frequency band tends toward classification of sediment type and/or texture analysis. For example, side-scan sonar, swath bathymetry and sub-bottom profilers are being used for seabed classification and bottom roughness estimation [10, 11]. There are also several commercial systems that process the backscattered returns from normal incidence echo-sounders for the purpose of sediment discrimination. These commercial systems fall into two categories: (1) Processing the echo to extract salient features that allow sediment discrimination [12] and (2) Processing the first and second backscatter from the sea floor to discriminate the sediment [13]. A theoretical basis for discrimination of sediment types using the energy densities of the first and second echo from the water/sediment interface (referred to as E_{s1} and E_{s2}, respectively) has been derived by Heald and Pace [14]. They show that whereas the E_{s1} return is clearly *monostatic*, the E_{s2} return must be treated with a *bistatic* geometry in which a virtual transmitter is located at a height of 2 to 3 water depths – the value being a function of the actual depth of the transmitter. The model is based on a Helmholtz-Kirchhoff development for scattering from a rough interface evaluated at normal incidence. Classification is achieved by combining information on the surface reflection coefficient obtained in the near-field, with surface roughness information obtained in the far-field [15]. Because it is a high frequency model, penetration into the seabed could safely be ignored.

In the present paper, we examine the feasibility of extending the model [14] down to the 1 – 10 kHz band.

TG Leighton, GJ Heald, HD Griffiths, G Griffiths, (eds.), 'Acoustical Oceanography', Proc. Institute of Acoustics Vol. 23 Part 2, 2001.

This would provide additional discrimination information since contributions from the seabed volume become significant. Additionally, it allows for information about the nature of seabed layers that may be present. However, all this comes at the cost of a more complicated model as well as a more complex data set. In addition to lowering the frequency we consider the impact of employing a vertical receive array which encompasses a substantial portion of the water column. This provides a series of near-field and far-field measurements using only the first bottom return and eliminates any degradation of the bistatic return that would result from sea-surface roughness.

Following the introduction, the model [14] shall be reviewed as background to the present work. Then the impact that lowering the frequency band will have on sediment classification will be examined. First, the simple case of a seabed consisting of an infinite inhomogeneous fluid half-space is considered. We then briefly examine modifications to the model to include scattering from a layer within that inhomogeneous volume. Finally, the advantages of employing a vertical receive array in place of a point receiver are considered.

2. Theoretical Background to the HF classification model

Since the current paper incorporates much of the work by Heald and Pace [14] we shall begin with a review of that model. Figure 1 contains a schematic of the intensity of the 1st and 2nd returns from the seabed interface (denoted I_{sb1} and I_{sb2}) from an echo-sounder. Whereas the geometry for the first return is clearly monostatic, the second return must be modeled as a vertically bistatic return with a virtual source located at height h_v above the sea surface. This is shown in Figure 2 in which the reflection from the sea surface has been unfolded to show the position of the virtual source. Note that the insonified area for the monostatic return, dA_1, will be in the far-field for all typical geometries. This is in direct contrast with the bistatic return in which the virtual source and the receiver are displaced such that $\theta_1 \neq \theta_2$ and one must employ a near-field model.

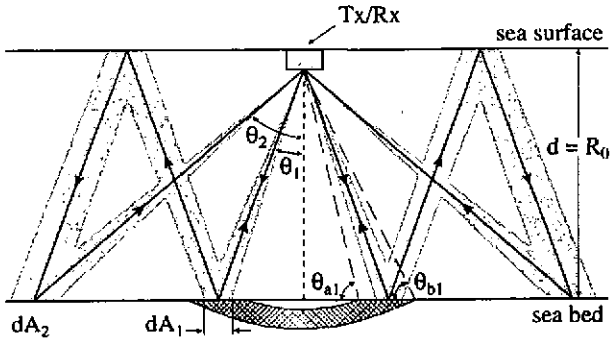

Figure 1. Cross-sectional schematic showing the paths of the 1st and 2nd returns from the seabed interface for a normal incidence echo-sounder. The hatched region represents the pulse as it propagates into the seabed. The shaded region represents an exaggerated view of the incremental angle $d\theta_1$. In the absence of volume scatter, only that portion of the pulse in contact with the interface contributes to the scattered intensity. For the 1st return this corresponds to the area constrained by $\theta_a > \theta_1 > \theta_b$.

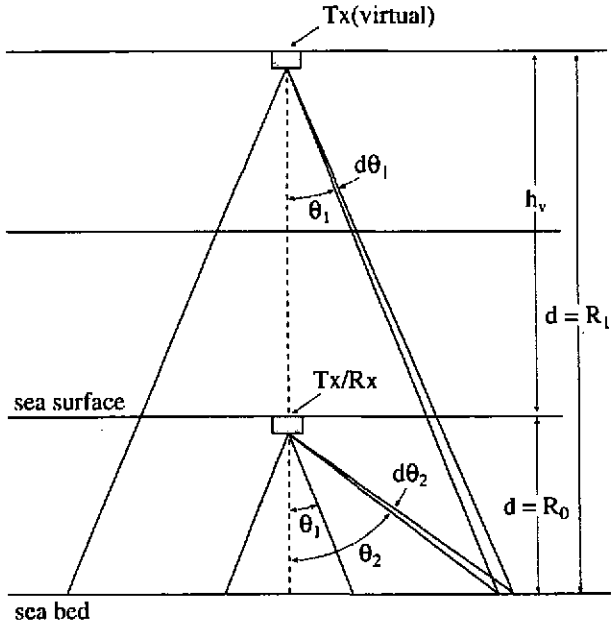

Figure 2. Schematic of the equivalent geometry with virtual source located at h_v above the sea surface.

Examining the monostatic return, we note that if the transducer is in the far-field of the incremental area dA_1 and the surface is sufficiently rough then the scattered field is incoherent and the intensity can be expressed as [14]:

$$I_{sb1} = I_o \int_{\theta_{a1}}^{\theta_{b1}} \frac{S_1(\theta_1) G_{Tx}(\theta_1) G_{Rx}(\theta_1)}{\left(R_o \sqrt{1+\tan^2(\theta_1)} \right)^4} dA_1 \qquad (1)$$

where G_{Tx} and G_{Rx} are the intensity beam patterns of the transmitter and receiver respectively, $S_1(\theta_1)$ is the surface backscattering coefficient given by

$$S_1(\theta_1) = \frac{\Re^2 T^2 \exp\left[-(T\tan\theta_1/2h)^2\right]}{32\pi h^2 \cos^4\theta_1} \tag{2}$$

where $\Re$ is the magnitude of the Rayleigh reflection coefficient, and h and T are the rms height and correlation length of the surface roughness (assumed isotropic). Integration of (1) yields

$$I_{sb1} = \frac{M}{2\beta^2}\exp\left[\frac{\beta^2 c(\tau - t)}{R_o} - 1\right] \tag{3}$$

where $M = I_o(\Re T/4hR_o)^2$ and $\beta^2 = (T/2h)^2 + 1/\tan^2\theta_b$ for an omnidirectional receiver and a transmitter with a Gaussian beam pattern in which θ_b corresponds to the 1/e point on the intensity beam function. The energy density E_{s1} of the first seabed return is then given by:

$$E_{s1} = \int_{t_1}^{\infty} I_{sb1}\,dt \tag{4}$$

where the subscript s denotes the surface of the seabed to distinguish it from the volume beneath the seabed, $t_1 = t_o + \tau$, and where t_o, τ are the onset of the return and the pulse duration, respectively. The integration is performed over only the tail of the return to avoid overload of the receive amplifier. For the bistatic return one integrates over the complete backscatter return to obtain [14]:

$$E_{s2} = \int_{t_o'}^{t_2} I_{sb2}\,dt + \int_{t_2}^{\infty} I_{sb2}\,dt \tag{5}$$

where $t_2 = t_o' + \tau$, t_o' is the onset of the bistatic return. The term I_{sb2} is given by [16]

$$I_{sb2} = \frac{\pi \Re^4 \beta_1^2}{4R_2^2\beta_4^2}\left[\exp(-x)\left(\left(\left[\frac{-1}{\left(x+\frac{1}{B_2}\right)}\right]+\left[\frac{1}{\left(x+\frac{1}{B_2}\right)^2}\right]\right)\left(1-\frac{2B_1}{B_2}+\frac{B_1^2}{B_2^2}\right)\exp\left(\frac{-1}{B_2}\right)+\left(\frac{-2B_1}{B_2}+\frac{B_1^2}{B_2^2}-\frac{xB_1^2}{B_2}-\frac{B_1^2}{B_2}\right)\right)\right]_{x_a}^{x_b} \tag{6}$$

where $\{x_a = 0,\ x_b = \theta_{a2}^2\beta_4^2\}$ for $t < t_o'$ and $\{x_a = \theta_{a2}^2\beta_4^2,\ x_b = (\theta_{a2} + \partial\theta)\beta_4^2\}$ for $t > t_o'$ and the terms B_1 and B_2 are defined in [16] of this Proceedings and are functions of T, h, θ_o and R_1/R_o. Note that the factor $\Re^4$ occurs because the scattered wave has undergone two (rather than one) seabed reflections.

As shown in [15] the average backscattered intensity measured in the near-field is proportional to the plane wave reflection coefficient for the surface, whereas in the far-field limit the backscattered intensity is inversely proportional to the mean square slope. Classification is achieved by contrasting the roughness and reflection properties of various sediment types [17].

In extending the model to low frequency, there is still one outstanding issue that should be addressed. With a monostatic geometry, it is impossible to distinguish between a signal scattered from within the seabed at normal incidence, and one scattered from a surface feature located at the appropriate slant range. This uncertainty is depicted in Figure 3 (in cross-section) by the circular arc; paths $\varepsilon_0\varepsilon_1\varepsilon_0$ and $\varepsilon_0\varepsilon_2\varepsilon_0$ have the same time of flight. Use of the bistatic return (i.e. I_{sb2}) alters the surface of time-coincident arrivals from a sphere to an ellipsoid. This allows one to separate surface scatter from a sub-bottom layer. This is depicted (in cross-section) by the ellipse in the figure and shows paths $\varepsilon_0\varepsilon_1\varepsilon_3\varepsilon_0$ and $\varepsilon_0\varepsilon_4\varepsilon_5\varepsilon_0$ which have the same time of flight. For further discussion of this see [18]. Of course, resolving layers from roughness features in this way requires the transducer to be well removed from the sea surface since the ellipse collapses to a circle as the transducer approaches the air-water interface. Next we extend the classification model to lower frequencies.

3 Extension of High-Frequency Classification model to Lower Frequency

In this section we examine the potential for extending the classification model to low frequency. In the present context, low-frequency implies that penetration into the seabed is significant. In practice this means that the contribution of volume scatter from within the seabed (and possibly the effect of sub-bottom layers) must be

included. Before proceeding it should be mentioned that Pouliquen *et al.* [19] have previously developed a sophisticated model for vertical incidence scatter from a Gaussian rough seabed which includes volume perturbations; however their model requires numerical solution. The present heuristic approach - although somewhat simplistic - has the advantage of being analytically solvable. We shall begin with the simplest scenario in which the seabed consists of an infinite inhomogeneous fluid half-space. To further simplify the development, we shall consider an omnidirectional receiver and an idealized source whose beam is of finite extent. The source is omnidirectional within $\theta < \theta_b$ and truncated outside this region.

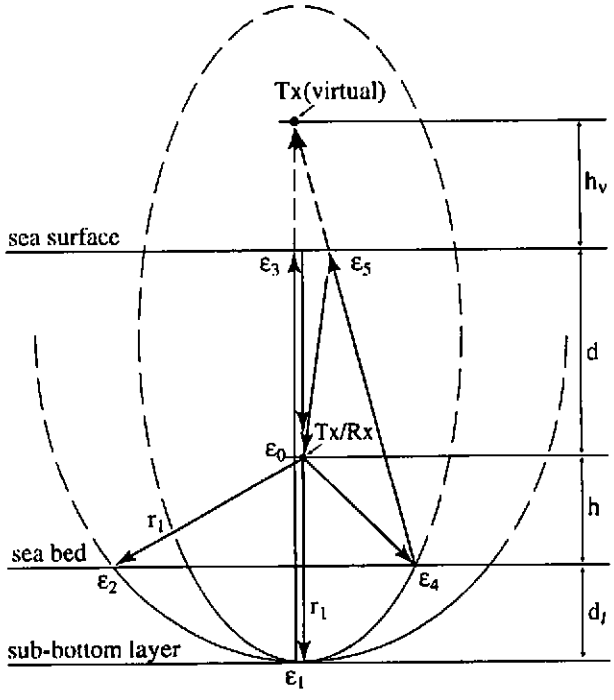

Figure 3. With a monostatic geometry, it is impossible to distinguish between a signal scattered from within the seabed at normal incidence, and one scattered from a surface feature located at the appropriate slant range. Using the bistatic return alters the surface of time-coincident arrivals from a sphere to an ellipsoid which allows one to separate surface scatter from a sub-bottom layer (see text).

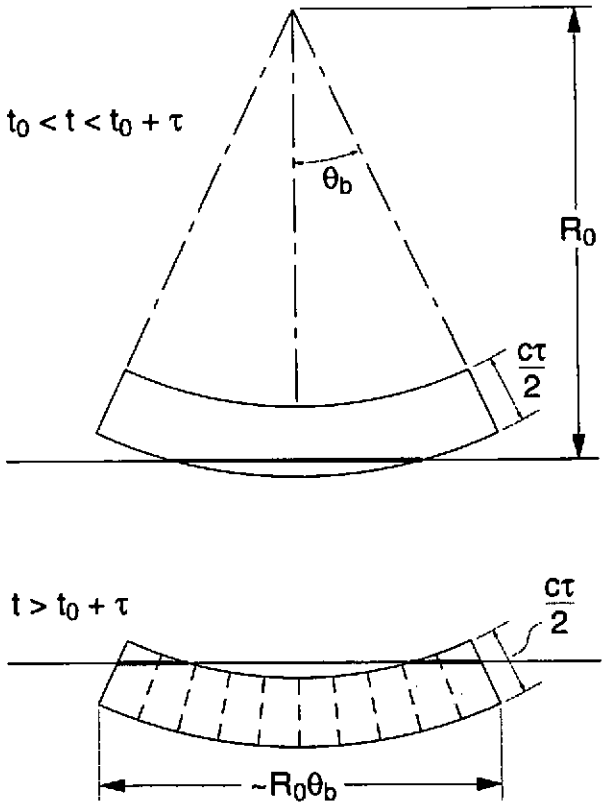

Figure 4. Cross-sectional schematic of the insonified volume using an idealized source. As the pulse reaches the seabed, the energy scattered from the interface increases as the surface contacted by the pulse grows (thick horizontal line). Later the insonified spot transitions to an annulus and the volume begins to contribute significantly to the total scattered energy.

3.1 Scattering contribution from the sub-bottom volume

Consider the idealized source with beamwidth θ_b and pulse duration τ incident on the bottom. Figure 4 shows a cross-sectional schematic of the insonified volume. As the pulse reaches the seabed, the energy scattered from the interface increases as the surface contacted by the pulse grows (thick horizontal line in Figure 4). This time corresponds to the rise of the I_{sb1} curve. At time $t_o + \tau$ after the pulse first comes in contact with the seabed, the insonified spot transitions to an annulus as the back of the pulse propagates into the bottom. This corresponds to the peak in the I_{sb1} curve. At time t_o, the volume begins to contribute to the total scattered energy (shaded area in Figure 4) and it reaches its maximum at approximately $t_o + \tau$ as the full pulse first intercepts the bottom. Scatter from the interface typically dominates the intensity during the time $t_o < t < t_o + \tau$; however, for low to moderate frequencies absorption in the seabed will be low and surface scatter will decay at a much faster rate than will the volume contribution. This will be demonstrated in the numerical examples and will be exploited for classification.

We begin by expressing the backscattering cross-section per unit volume, σ_v, in the form [20]:

$$\sigma_v = \frac{\pi}{2}|k_s|^4 \Phi(k_s) \tag{8}$$

where k_s is the acoustic wavenumber in the seabed, and $\Phi(k_s)$ is the three-dimensional spectrum of the seabed heterogeneities defined in terms of fluctuations in acoustic impedance. The function $\Phi(k_s)$ is given by the Fourier transform of the correlation function of the heterogeneities, $N(r)$, and in the far-field reduces to:

$$\Phi(k_s) = \int_{x,y,z} N(r)\exp(ik_s \cdot r)dxdydz \tag{9}$$

where r is the relative displacement given by $r = \hat{i}x + \hat{j}y + \hat{k}z$. Several expressions for $\Phi(k_s)$ have been evaluated [21, 22] based on various models for the correlation function $N(r)$. When numerically evaluating (9) we shall assume the simplified power law form given in [22]:

$$\Phi(k) = \frac{A_v / 2\pi}{\left(K^2 p^2 + q_z^2 + L_z^{-2}\right)^{3/2}} \tag{10}$$

where A_v is proportional to the mean square value of the spectrum strength of the heterogeneities, L_z is the vertical correlation length scale, p is the aspect ratio of horizontal to vertical correlation length, and K and q_z are the horizontal and vertical components of the scattered wavenumber vector. The maximum intensity of the volume scatter, measured by a source/receiver located in the far-field at height R_o above the seabed is then:

$$I_{v\max} \approx V\frac{I_o}{R_o^4}(1+\Re)^4\left(\frac{\rho_w}{\rho_s}\right)^2\frac{\pi}{2}|k_s|^4\Phi(k_s) \tag{11}$$

where V is the insonified volume, I_o is the incident source level measured 1 m from the source, the term $(\rho_w/\rho_s)^2(1+\Re)^4$ accounts for the two-way transmission through the interface, ρ_w, ρ_s are the water and sediment densities, respectively, and it is assumed that the pulse length is short enough to neglect absorption when computing $I_{v\max}$. We cannot directly apply (11) to the present problem because $\Phi(k_s)$ is a far-field solution whereas the source (by virtue of its finite beamwidth) is in the near-field. However, we can obtain an approximate solution to the scattered intensity by sectioning the volume contiguously such that each sub-volume is in the far-field of the receiver. That is to say, across any given sub-volume the angle θ is approximately constant. This is represented in Figure (4) using the dashed lines in the insonified volume. Implicit in this approximation is the assumption that the correlation length of the heterogeneities is significantly smaller than the width of any sub-volume. This will ensure that the effect of contributions from adjacent edges of the sub-volumes is small compared to the total scattered intensity. These edge effects should average out in any case since they only contribute to the coherent (rather than incoherent) component of the total intensity. In the limit one obtains

$$I_{v\max} \approx \frac{I_o}{R_o^2}\left(\frac{\rho_w}{\rho_s}\right)^2\pi^2\frac{c\tau}{2}|k_s|^4\int_0^{\theta_b}[1+\Re(\theta)]^4\Phi(k_s)\sin(\theta)d\theta. \tag{12}$$

which amounts to averaging the scattered intensity across incidence angle. To compute I_{vb1} it is necessary to account for the time dependence of the scattered intensity. Absorption in the seabed will result in an exponential decay of the intensity so that we have:

$$I_{vb1} \approx I_{v\max}\exp\{-4\alpha[c_s(t-t_o)/2]\}. \tag{13}$$

where α is the absorption in nepers/m, $c_s(t - t_o)/2$ is the one-way path length in the bottom, and the factor of 4 accounts for the two way path length in the sediment *and* the conversion from pressure to intensity. The reader may have noted that this formulation assumes that the transmitted plane wave propagates *coherently* whereas the reflected wave was previously assumed to scatter *incoherently*. This apparent dichotomy can be rectified by examining the roughness parameter for the reflected (g_r) and the transmitted (g_t) waves. From [23] one obtains:

$$g_r = \{k_w h[\cos(\theta_i)+\cos(\theta_r)]\}^2,\ g_t = \{k_w h[\cos(\theta_i)-n\cos(\theta_t)]\}^2 \tag{14a}$$

where the subscripts i, r, and t denote incident, reflected and transmitted angles measured from vertical, k_w is the acoustic wavenumber in water, n is the index of refraction, and h is the rms roughness. For normal incidence this simplifies to:

$$g_r = (2k_w h)^2,\ g_t = [k_w h(1-n)]^2. \tag{14b}$$

From (14a,b) we note that whereas g_r is proportional to the roughness and the wavenumber, g_t is proportional to

the roughness and the *change* in wavenumber (through the term 1-n); since $\Delta k << k_w$ the transmitted wave is much more coherent than the reflected wave. This effect of roughness is illustrated qualitatively in Figure 5. The two points on the plane wave front incident on the bottom undergo a relative phase change of $2k_w\Delta h$ upon reflection. For the same two points, the change in phase of the transmitted wave is only $\Delta k_w\Delta h$ as the wave propagates into the seabed at a slightly faster wave speed. As k_s approaches k_w the apparent roughness of the boundary goes to zero and the transmitted wave propagates undistorted as expected. It is interesting to note that for the reflected wave the boundary still appears rough even for $k_s = k_w$; it is the *magnitude* of the reflection coefficient that goes to zero. This is a simplified interpretation of course which doesn't account for effects such as refraction due to the local angle of incidence. In fact, the roughness parameter enters not as a phase term but as a multiplier which acts to reduce the coherence of the wave. This occurs through the factor $\exp(-g_m)$ where $m = r$ or t. When $\exp(-g_m) = 1$ the wave is fully coherent and when $\exp(-g_m) = 0$ the wave is fully incoherent. Figure 6 contains a plot of the function $\exp(-g_m)$ with $n = 0.93$ for two substantially different values of roughness. The figure clearly indicates a coherent transmitted wave and a predominately incoherent reflected wave over most of the frequency band of interest.

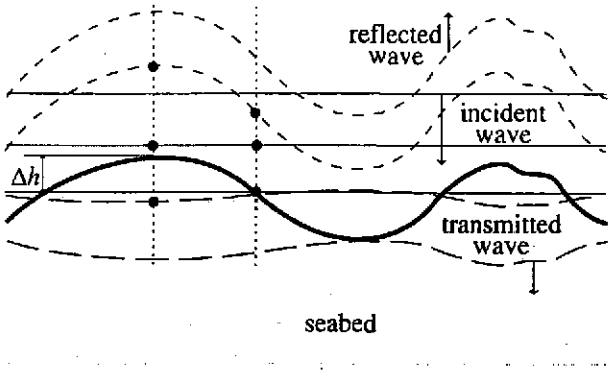

$\Delta\psi_{ir} = 2k_w\Delta h, \quad \Delta\psi_{it} = \Delta k\Delta h$

$\Delta k = k_w - k_s, \quad \Delta k << k_w$

Figure 5. Qualitative illustration of normal incidence plane wave being reflected and transmitted at a rough boundary. The reflected wave front undergoes significantly more distortion than the transmitted wave front.

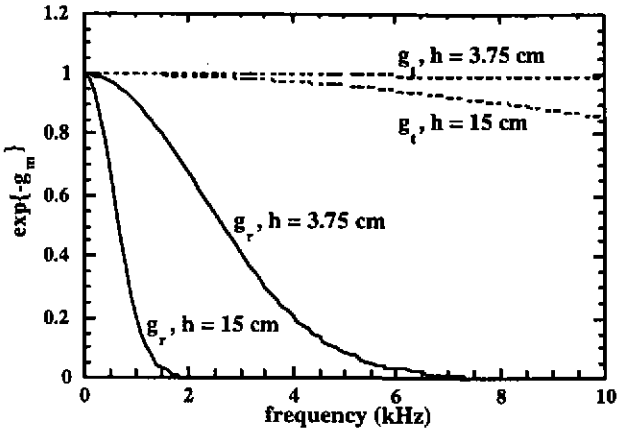

Figure 6. Coherence of reflected and transmitted wave generated by a normal incidence plane wave intercepting a rough boundary. A value of unity implies the wave will be coherent; conversely a value of 0 implies the wave will be incoherent.

Figures 7 and 8 show the time dependence of I_{sb1} and I_{sb2} plotted in decibels, for a silt bottom and a sand bottom assuming a 5 ms pulse. The plots are done using several values of rms roughness h with the surface correlation fixed at $T = 1.5$ m. The physical constants for silt and sand required to evaluate I_{sb1} and I_{sb2} were taken from [22]. Note that $t = 0$ for curve I_{sb1} corresponds to $t = t_0$ whereas $t = 0$ for curve I_{sb2} corresponds to $t = t_0$'. The time scales of the two sets of curves have been overlayed to allow comparison. In the absence of sub-bottom scatter, one integrates I_{sb1} and I_{sb2} and classification is achieved because the relative values of E_{s1} and E_{s2} are reasonably distinctive for different sediment types – the sand and silt curves merely serving as examples.

Figures 9 and 10 shows the time dependence of I_{vb1} plotted in decibels, for a silt bottom and a sand bottom at 1, 5, and 10 kHz. Values of $p = 5$, $L_z = 1$, and $A_v = 0.001$ along with the physical constants from [22] were used to evaluate I_{vb1}. The curves for I_{sb1} are replotted from Figures 7 and 8 for comparison. The first feature to note is that the maximum intensity and the time dependence of I_{vb1} depend on both frequency and sediment type. Furthermore, although surface scatter initially dominates the return, the high rate of decay of the surface scatter results in volume scatter dominating the return less than 5 ms after the peak intensity. One could use the change in slope to mark the transition to volume-dominated scatter, and the level as an indicator of the type of sediment. Clearly a wide frequency band source would assist in classification given the frequency dependence of the volume scatter.

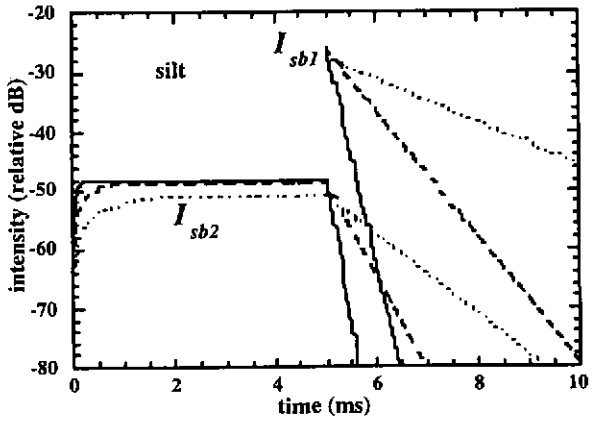

Figure 7. Comparison of I_{sb1} and I_{sb2} for a silt bottom for rms roughness h = 3.75 cm (solid line), 7.5 cm (dash line), and 15 cm (dotted line). For all curves the correlation length is T = 150 cm.

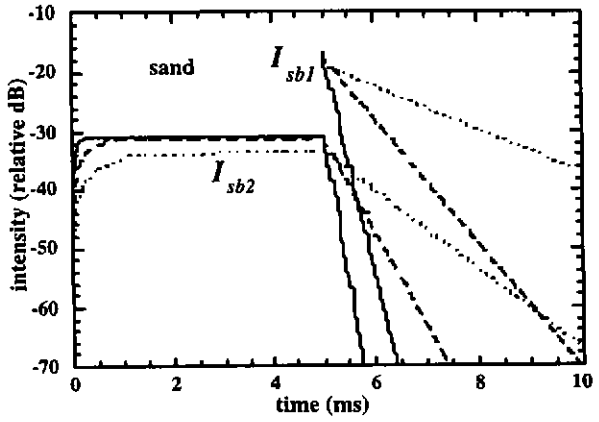

Figure 8. Comparison of I_{sb1} and I_{sb2} for sand bottom for rms roughness h = 3.75 cm (solid line), 7.5 cm (dash line), and 15 cm (dotted line). For all curves the correlation length is T = 150 cm.

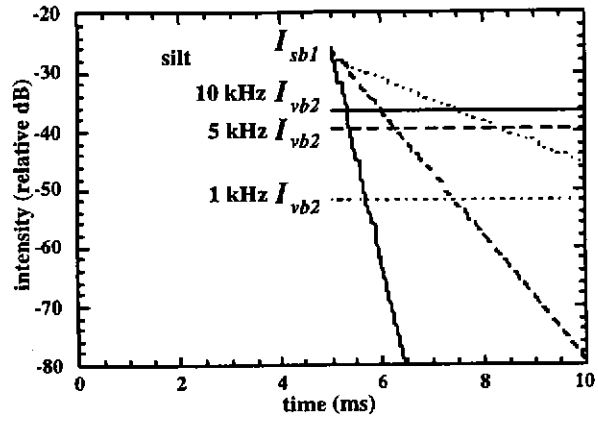

Figure 9. Comparison of I_{sb1} and I_{vb1} for a silt bottom for rms roughness h = 3.75 cm (solid line), 7.5 cm (dash line), and 15 cm (dotted line), at frequencies of 1, 5, and 10 kHz.

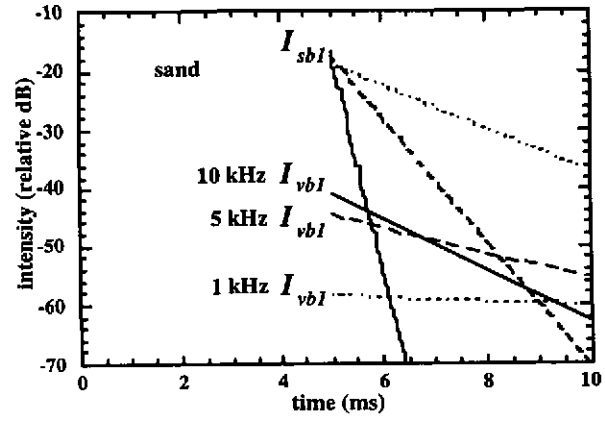

Figure 10. Comparison of I_{sb1} and I_{vb1} for a sand bottom for rms roughness h = 3.75 cm (solid line), 7.5 cm (dash line), and 15 cm (dotted line), at frequencies of 1, 5, and 10 kHz.

Furthermore, if one alters the integration time when computing E_{s1} such that

$$E_{s1} \approx \int_{t_1}^{t_3} I_{sb1} dt \tag{15}$$

where t_3 corresponds to the time of the change in slope, then for the examples cited here E_{s1} is within 10% of that obtained using (4). This means that volume scatter has virtually no negative impact on the surface scatter classification technique while providing additional classification information.

3.2 Scattering from a sub-bottom layer

At low frequency it is not uncommon for the layered structure of the seabed to become apparent. For this reason we shall briefly consider the possibility of modeling a buried layer. We begin by expressing the intensity incident at a sub-bottom layer, I_l, located d_l below the water/sediment interface as:

$$I_l \approx \frac{I_o \cdot (1+\Re)^2 \exp(-2\alpha d_l)}{R_o^2[1+\tan^2(\theta_1)]} \tag{16}$$

where we assume $R_o >> d_l$ and the exponential term accounts for absorption in the overlying sediment *for the down-going propagation path only*. The backscattering coefficient for the sub-bottom layer will be of the same form as that of the interface with the factors $\Re_l$, T_l, and h_l referring to the sub-bottom layer; also, θ_1 is replaced with θ_{l1} where $\sin(\theta_{l1}) = \sin(\theta)/n$ and $\cos^2(\theta_{l1})=1-\sin^2(\theta_1)/n^2$ and n is the index of refraction for the two sediment

types.

This leads to the following expression for the monostatic backscattering coefficient at the sub-bottom interface:

$$I_{lsb1} = I_o \cdot \left(\frac{\rho_w}{\rho_s}\right)^2 (1+\Re)^4 \exp(-4\alpha d_l) \int_{\delta\theta_{l1}} \frac{S_{l1}(\theta_{l1}) G_{Tx}(\theta_1) G_{Rx}(\theta_1)}{\left(R_o \sqrt{1+\tan^2(\theta_1)}\right)^4} dA_{l1} \tag{17}$$

where the subscript l refers to the sub-layer and S_{l1} is given by:

$$S_{l1} = \frac{\Re_l^2 T_l^2}{32\pi h_l^2} \cdot \left(\frac{\exp\left[-\left(\frac{T_l \theta_1}{2nh_l}\right)^2\right]}{\left[1-(\theta_1/n)^2\right]^2} \right) \tag{18}$$

and we have made the narrow beamwidth approximation $\tan(\theta) \approx \sin(\theta) \approx \theta$. The expression for I_{lsb2} can be obtained in a similar manner.

4. The Effect of a Vertical Line Array Receiver

Up to this point the model has assumed a co-located source and receiver. This has certain engineering advantages since the water-borne portion of the system is compact and signal processing requirements are small. That said, if one can accept the added complexity, a vertical line array receiver would improve sediment classification considerably. The vertical aperture would enable a series of measurements which would transition from near-field bistatic (using the hydrophone nearest the seabed) to far-field monostatic (using the hydrophone co-located with the transmitter) [15]. In addition, the line array eliminates the requirement for the surface reflected path which is sea-state dependent. Alternatively, the array aperture can be used to steer beams at or near vertical incidence to separate shallow angle surface returns from sub-bottom layers [24]. However this restricts the frequency band due to the nature of line array processing. In any case, the bi-static returns to the individual elements can be can be used to isolate surface from sub-bottom using a procedure similar to that depicted in Figure 3.

5. Concluding Remarks

In this paper we have extended a high-frequency model for sediment classification down to lower frequency. In the present context lower frequency implies that scatter from the sub-bottom volume must be included. Although scatter due to seabed roughness initially dominates the return, its high rate of decay results in volume scatter dominating the return at longer times. One can use the change in slope of the decay to mark the transition to volume-dominated scatter, and the level as an indicator of the type of sediment. Furthermore, a wide frequency-band source would assist in classification since the volume scatter exhibits a marked dependence on frequency. A formulation to extend the model to include scatter from a buried layer was examined briefly and appears feasible. Finally, a vertical line array – as opposed to a single receiver co-located with the transmitter– would significantly improve sediment classification at the cost of increasing the system's complexity.

6. Acknowledgements

The authors wish to acknowledge the insight provided by Dr. Nick Pace of SACLANT Centre, Dr. John Osler and Dr. David Thomson of DREA and Dr. Anatoliy Ivakin of the Andreev Acoustics Institute.

References

[1] Fortuin, L. Survey of literature on reflection and scattering of sound waves at the sea surface. *J. Acoust. Soc. Am.*, 1970; **47**: 1209-1228.

[2] Chapman RP, Bluy OZ, Hines PC. Backscatter from rough surfaces and inhomogeneous volumes. *in* Encyclopaedia of Acoustics, edited by MJ. Crocker. Wiley-Interscience, New York, 1997, pp. 441-458.

[3] Ivakin AN. A unified approach to volume and roughness scattering. *J. Acoust. Soc. Am.*, 1998; **103**: 827-837.

[4] Buker HP. Use of calculated sound fields and matched-field detection to locate sound sources in shallow

water. *J. Acoust. Soc. Am.*, 1976; **59**: 368-373.

[5] Collins MD and Kuperman WA. Focalization: environmental focusing and source localization. *J. Acoust. Soc. Am.*, 1991; **90**: 1410-1422.

[6] Gerstoft P. Inversion of seismoacoustic data using genetic algorithms and a posteriori probability distributions. *J. Acoust. Soc. Am.*, 1994; **95**: 770-782.

[7] Holland CW, Osler J. High-resolution geoacoustic inversion in shallow water: a joint time- and frequency-domain technique. *J. Acoust. Soc. Am.*, 2000; **107**: 1263-1279.

[8] Diachok O, Caiti A, Gerstoft P, and Schmidt H. (Editors) Full Field Inversion Methods in Ocean and Seismo-acoustics. Ed., Kluwer Academic, Dordrecht, 1995.

[9] Wilson JH, Rajan SD, and Null JM. (Editors) Inversion Techniques and the Variability of Sound Propagation in Shallow Water. Special Issue *J. Oceanic Eng.* 1996; **21**: 321-504.

[10] Goff JA, Swift DJP, Duncan CS, Mayer LA, and Hughes-Clarke J. High-resolution swath sonar investigation of sand ridge, dune and ribbon morphology in the offshore environment of the New Jersey margin. *Marine Geology*, 1999; **161**: 307-337.

[11] Lambert DN, Walter DJ, Young DC, Griffin SR, and Benjamin KC. Developments in acoustic sediment classification, Proceedings: IEEE Oceans'98, 1998; pp. 26-31.

[12] Preston JM, Rosenberger A, and Collins WT. Bottom classification in very shallow water. Proceedings: 5th European Conference on Underwater Acoustics, edited by ME Zakharia, Lyon, France, 2000, pp. 293-299.

[13] Chivers RC, Emerson N, and Burns DR. New acoustic processing for underway surveying. *Hydrographic Journal*, 1990; **56**: pp. 9-17.

[14] Heald GJ, and Pace N.G. An analysis of 1st and 2nd echoes for seabed classification., in *Proceedings: 3rd European Conference on Underwater Acoustics*, JS Papadakis (ed.). Forth-IACM, Heraklion, 1996, pp. 649-654.

[15] Pace NG, AL-Hamdani ZKS, Thorne PD. The range dependence of normal incidence acoustic backscatter from a rough surface, *J. Acoust. Soc. Am.*, 1985; **77**: 101-112.

[16] Heald GJ. High frequency sea bed backscattering and sediment discrimination, in *'Acoustical Oceanography', Proceedings of the Institute of Acoustics Vol. 23 Part 2, 2001*, T G Leighton, G J Heald , H Griffiths and G Griffiths, (eds.), Institute of Acoustics, (this volume), pp. 258-267.

[17] Heald GJ and Pace NG. Implications of a bi-static treatment for the second echo from a normal incidence sonar, Proceedings: 13th World Congress on Acoustics and 135th meeting of the Acoustical Society Of America, edited by PK Kuhl and LA Crum. ASA, 1998; 3009-3010.

[18] Hines PC, Crowe DV, and Ellis, DD. Extracting in-plane bistatic scattering information from a monostatic experiment. *J. Acoust. Soc. Am.*, 1998; **104**: 758-768.

[19] Pouliquen E, Bergem O, and Pace NG. Time-evolution modeling of seafloor scatter. I. Concept. *J. Acoust. Soc. Am.*, 1999; **105**: 3136-3141.

[20] Ivakin AN. High frequency scattering from heterogeneous seabeds. Proceedings: 5th European Conference on Underwater Acoustics, edited by ME Zakharia, Lyon, France, 2000, pp. 1241-1246.

[21] Hines, PC. Theoretical Model of Acoustic Backscatter From a Smooth Seabed. *J. Acoust. Soc. Am.*, 1990; **88**: 324-334.

[22] Ivakin AN. Models for seafloor roughness and volume scattering. Proceedings: Oceans'98, Nice, France, 1998, pp. 518-521.

[23] Medwin H and Hagy JD. Helmholtz-Kirchhoff theory for sound transmission through a statistically rough plane interface between dissimilar fluids. *J. Acoust. Soc. Am.*, 1972; **51**: 1083-1090.

[24] Tang D, Frisk, GV, Sellers J, and Li D. Low-frequency acoustic backscattering by volumetric inhomogeneities in deep-ocean sediments. *J. Acoust. Soc. Am.*, 1995; **98**: 508-516.